PHILOSOPHICAL TRANSACTIONS OF THE ROYAL SOCIETY A MATHEMATICAL, PHYSICAL & ENGINEERING SCIENCES

The surface activity of ultrafine particles

D. A. Jefferson

Phil. Trans. R. Soc. Lond. A 2000 **358**, 2683-2692
doi: 10.1098/rsta.2000.0677

10.1098/rsta.2000.0677

THE ROYAL SOCIETY

The surface activity of ultrafine particles

By D. A. Jefferson

University Chemical Laboratories, Lensfield Road, Cambridge CB2 1EW, UK

Within the last 20 years, advances in characterization methods, particularly in the field of high-resolution electron microscopy, have made it possible to probe the surface and internal structure of sub-100 nm particles, or nanoparticles. Such studies have indicated conclusively that surface-energy considerations in metal nanoparticles cause these particles to adopt structures which only approximate to close packing but are terminated by close-packed faces. In oxides, where stoichiometry must be maintained, the adoption of low-index crystallographic faces almost invariably necessitates the introduction of cation or anion vacancies, and both have been observed. In such cases, the structure at the edges of the particles differs greatly from that of bulk phases, and it seems highly probable that the physical and chemical properties of these particles are also different. In certain cases it appears that new structural types, found only in nanoparticulate form, may exist. The significance of these findings, particularly as regards their relevance to particulate pollutants in the atmosphere, may be of great interest.

Keywords: particle size; nanoparticle chemistry; particulate pollutants; nanoparticle structure

1. Introduction

The toxicological effects of ultrafine particles present in the atmosphere depend on many factors, both physical and chemical. Possibly the most important factor, apart from their concentration, is the size of the particles, as this determines where they are deposited in the respiratory tract and, hence, the manner in which they may interact with living tissue. Particle size is also crucial, as this is the main factor governing their removal from the atmosphere by filtration. However, the chemistry of such nanoparticles is also a factor to be considered. Although it has been shown that relatively inert materials have enhanced toxicological effects when present as sub-100 nm particles, implying that physical size is the main factor determining interaction with lung tissue (Amdur *et al*. 1988; Gilmour *et al*. 1997), it has also been suggested that the greater specific surface of such particles may raise kinetically or thermodynamically unfavourable reactions to significant levels. However, the relevant chemical properties of these particles have always been assumed to be those of the bulk material: for this reason, chemical action by sub-100 nm particles of inert oxides such as titania and alumina has generally been disregarded.

The high surface area—or, more correctly, the enhanced ratio of surface to bulk atoms—is the dominant factor in all nanoparticle properties. This has long been realized in the field of heterogeneous catalysis, where economic factors frequently necessitate the use of catalytic species in a finely divided particulate form. The importance of surface effects can be readily seen when metal nanoparticles are exposed to

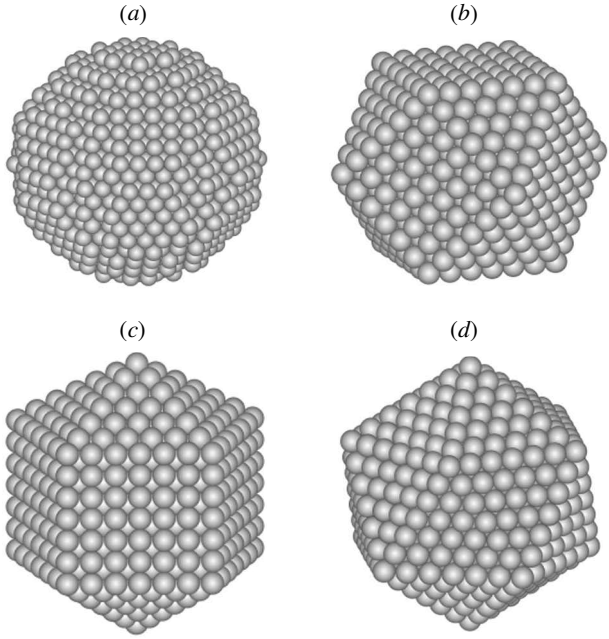

Figure 1. Models of the common morphologies adopted by metal nanoparticles: (*a*) spherical, (*b*) cubeoctahedral, (*c*) decahedral, (*d*) icosahedral.

an environment where stable surface adsorbate layers are formed: formation of the adsorbate can frequently provide enough energy for the complete reconstruction of the particles into a new morphology (Harris 1986; Jefferson & Harris 1988; Gribelyuk *et al*. 1994). As part of the search for increased catalyst efficiency, many structural investigations of nanoparticulate species have been performed, and these indicate that the small size and high proportion of surface atoms may have a profound effect on the internal structures of such particles, so much so that nanoparticles may differ appreciably from bulk material. The toxicological consequences of these differences may well be significant.

2. Metal nanoparticles

The simplest examples come from metals with the face-centred cubic structure. In order to minimize surface energy, it can be expected that nanoparticles will try to assume a shape which approximates to a sphere, as shown in figure 1*a*. In a close-packed metal structure, this is relatively easy, but for small particles the surface is marked by numerous steps, where the local coordination number is low and the energy is markedly raised from that of a bulk atom, which is 12-coordinated. A more stable surface can be created by using low-index crystallographic planes, such as {111} and {100}, to create a cubeoctahedral particle, shown in figure 1*b*. Here, the coordination numbers of atoms in these two surfaces are nine and eight, respectively, and although the surface area for a given number of atoms is increased, the overall energy is greatly reduced. Such faceted particles have been observed using high-resolution electron microscopy (Heinemann *et al*. 1979), but other more complex shapes have also been noted, particularly the so-called multiply twinned particles

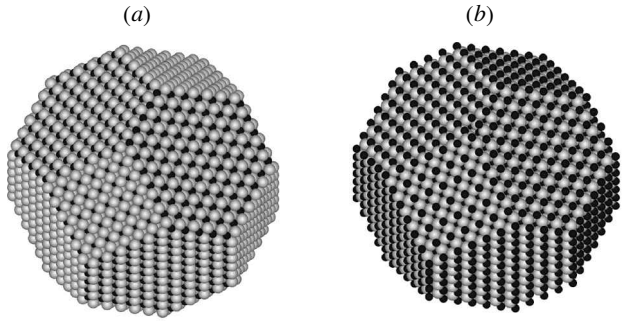

Figure 2. The stoichiometry problem faced by cubeoctahedral nanoparticles of CeO_2: (*a*) oxygen terminated, with composition $Ce_{2735}O_{5688}$; (*b*) metal terminated, with composition $Ce_{2735}O_{4600}$. In both cases cerium atoms are depicted by the small dark circles, with oxygen being the larger, lighter circles.

(MTPs) (Marks & Smith 1981, 1983). These, which comprise either decahedral or icosahedral particles (figure 1*c*, *d*) increase the ratio of the higher-coordinated {111} surfaces relative to the {100} type by twinning the structure such that each particle is made up of a number of smaller regions, numbering five in the decahedron and 20 in an icosahedron, the latter having only {111} surfaces.

It is relatively easy to show that decahedral and icosahedral configurations are much more stable than a simple spherical particle in both metal and non-metallic systems (Uppenbrink *et al*. 1992). However, there are subtleties in these structures which are not immediately apparent. If the face-centred cubic structure is twinned on the {111} planes, as must happen in these MTPs, the angle between twin-related rows of atoms is 70.52°, whereas the geometry of the particle requires a 72° angle. The MTPs are, therefore, not compatible with a truly close-packed structure, and some strain must exist, as atom–atom separations parallel to the particle faces must be greater than their radial equivalents. Whether this strain is either accommodated homogeneously or concentrated near the twin boundaries has not been completely resolved (Howie & Marks 1984), although there is more evidence for the latter mechanism, but what is beyond doubt is that the stable, close-packed structure is relaxed to comply with surface requirements.

3. Oxide nanoparticles with anion vacancies

Many oxides are based upon approximately close-packed arrangements of oxygen anions, and similar behaviour might be expected in oxide nanoparticles, but when more than one type of atom is involved, a more important consideration becomes paramount, namely that of maintaining the oxide stoichiometry. A very simple example is given by the case of ceria, CeO_2, which is of considerable commercial importance as a catalyst support and oxygen storage medium, and is particularly easy to prepare in sub-10 nm form (Brinker & Scherer 1990). Ceria has the fluorite structure, and in nanoparticle form adopts a cubeoctahedral morphology, showing {111} and {100} surfaces, presumably to minimize surface-energy effects. However, the atomic arrangement on crystallographic planes with either of these sets of indices alternates between metal atoms and oxygen atoms, but no single plane contains both. A nanoparticle of ceria is therefore faced with an impossible dilemma, in that if it is

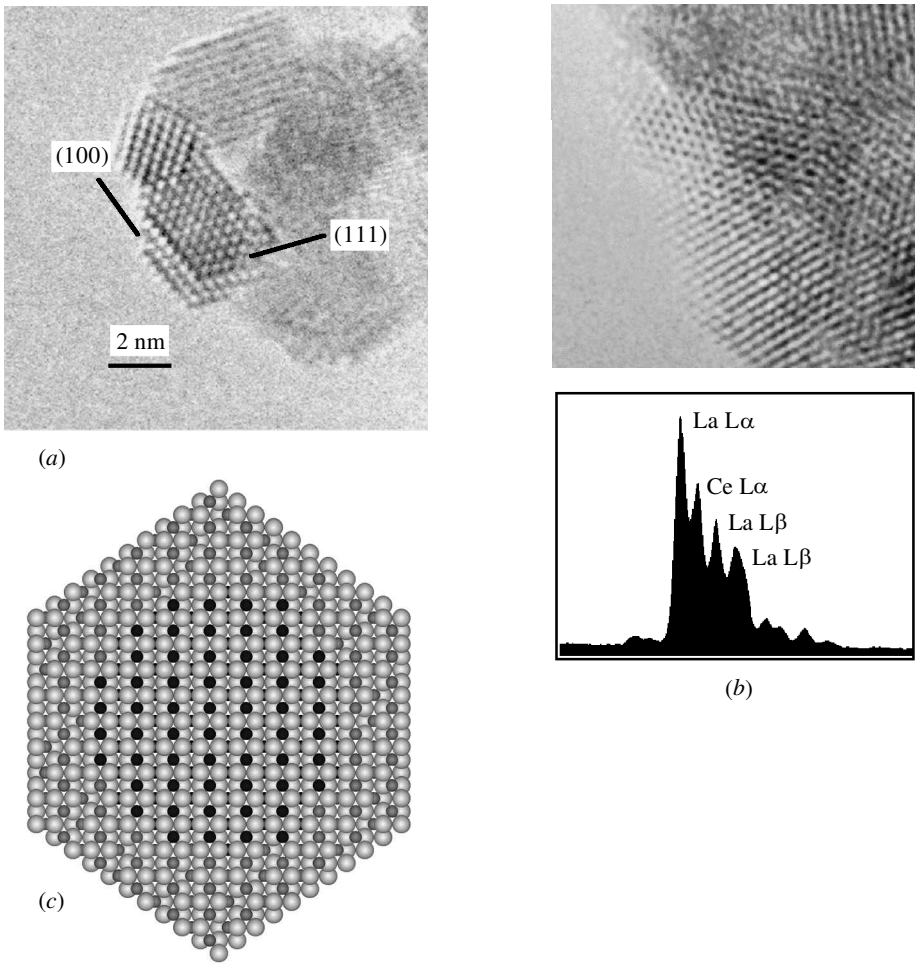

Figure 3. (*a*) High-resolution electron micrograph of a typical cubeoctahedral particle of CeO_2. (*b*) A less well-defined particle, but with the X-ray emission spectrum shown. (*c*) Schematic of a particle of CeO_2 coated with La_2O_3. Oxygen atoms are shown as large circles, with cerium being the small dark circles and lanthanum the small lighter ones.

terminated with planes of metals atoms, there is an excess of metal in the particle, but if oxygen termination is selected, there is an equal excess of oxygen. These two arrangements are shown schematically in figure 2.

The simplest way to overcome the problem of the surface excess of metal or oxygen atoms is to introduce vacancies of the opposite species within the bulk. High-resolution electron micrographs of ceria (figure 3*a*) do not appear to indicate any significant metal vacancies, as a regular array of metal atoms is clearly visible, but cerium does form a series of reduced oxides, which are based on regular arrangements of oxygen vacancies within the fluorite structure (Brauer 1964; Bevan 1973), so the presence of the latter is most likely, inferring a metal atom termination of the particles, although this cannot be substantiated by high-resolution electron microscopic studies, as the scattering from the oxygen is minimal at current resolution limits.

Consequently, no conclusions can be made concerning the location of such vacancies, if they are present.

Ceria is known to form solid solutions with many other metal oxides, particularly if they possess similar structures, and an excellent example of this is given by the solid solution with lanthana, La_2O_3. Lanthana normally adopts a hexagonal structure, but a cubic form is also known (Gschneider & Eyring 1979) and is based on an oxygen-deficient fluorite arrangement. Depending on the temperature of preparation, solid solubility of lanthana in ceria may extend up to more than 50% (Bevan 1955; Morris *et al.* 1993), and similar behaviour has also been found in mixed nanoparticles prepared by sol-gel methods (Tilley 1997). In the latter case, however, the limits of solid solubility are extended considerably, with two-thirds replacement of cerium by lanthanum being confirmed by microanalysis, although electron microscopic images indicate apparently normal ceria particles (figure 3*b*). Analysis of the surface composition of a specimen of uniformly sized particles using X-ray photoelectron spectroscopy, however, indicates a large preponderance of lanthanum atoms at the surface, although a high oxygen signal suggests that the surfaces are by no means metal terminated. These results can be reconciled with a model of the particles which is principally normal ceria in the interior, but then accommodates an increasing number of lanthanum atoms at or near the surfaces, with ordered oxygen vacancies (as found in cubic La_2O_3) located at the particle surfaces. This is illustrated schematically in figure 3*c*. This implies that particles of pure ceria may well behave in a similar manner, and consequently the surfaces of such particles might possess a reactivity not normally associated with the bulk oxide. This could explain the apparent ease with which ceria nanoparticles seem to dissolve other metals, as has been observed in electron microscopic studies (Hutchison 1990).

4. Oxide nanoparticles with cation vacancies

Oxides with the spinel structure, notably γ-alumina and Fe_3O_4, have exactly the same problems as ceria when produced in nanoparticle form, as they adopt either octahedral or cubeoctahedral morphologies, and although the structure is different, low index planes still contain either metal or oxygen atoms. In their case, however, the solution to the problem is very different. Nanoparticles of Fe_3O_4, which form the precursor of several types of iron catalyst, show remarkable features when observed in the electron microscope. One such image is shown in figure 4*a*, where a particle is observed at the margins of a much larger crystal, and it is notable in having well-defined edges (corresponding to projections of the {111} and {100} faces), although the particle interior gives the contrast normally expected from an amorphous material, implying a completely disordered arrangement. Such an arrangement, however, is not compatible with well-defined faces, and, in addition, clear contrast from the metal atoms is observed at the particle edges, although not elsewhere.

This paradox of an apparently amorphous particle with well-defined edges may be resolved by considering the stoichiometry problem. Unlike CeO_2 there is no way to incorporate vacancies into the close-packed arrangement of oxygens without breakdown of the structure, but cation vacancies are certainly possible, as are present in the defect spinel structure of γ-Fe_2O_3. If these nanoparticles are therefore terminated by planes of iron atoms, the resulting metal atom excess can be compensated for by the creation of metal vacancies in the interior. The anion sub-lattice remains intact,

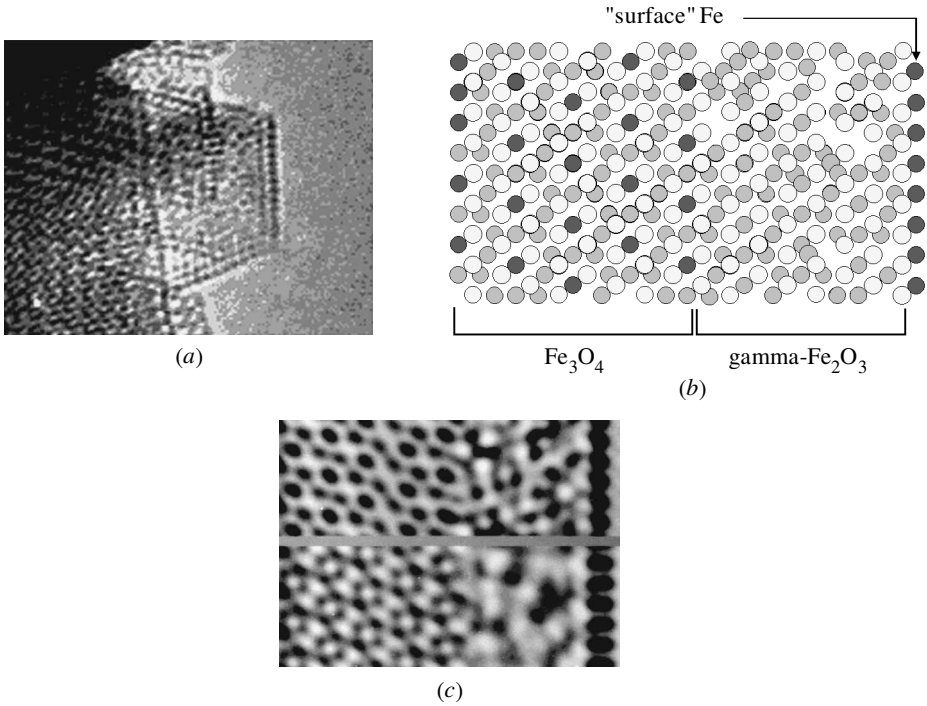

Figure 4. (*a*) High-resolution electron micrograph of a nanoparticle of iron oxide on the surface of a larger crystal of magnetite. (*b*) A model of the particle/substrate relationship, showing disordered metal vacancies in the nanoparticle with ordered metal atoms at the surface. The oxygen framework is shown as light circles, with single iron atoms as darker circles. Pairs of iron atoms projecting above one another are shown in the darkest shading. (*c*) Computer simulated image, showing enhanced contrast at the particle edge.

preserving the particle shape and morphology, but because the oxygens contribute only weakly to the overall image contrast, this regular component of the structure is not observed, and all that can be seen is the random arrangement of metal atoms, which will therefore appear amorphous. This hypothesis may be tested by constructing a model of regular Fe_3O_4 with a surface terminating in a plane of metal atoms, filling all the surface metal sites, and creating random metal vacancies in the subsurface layer to maintain the stoichiometry (figure 4*b*). The images simulated from this model (figure 4*c*) using the multislice method (Cowley & Moodie 1957) reproduce the experimental image contrast very well, indicating the basic soundness of this structural principle. Perhaps the most important feature is that to obtain sufficient contrast at the surface layer, it is necessary to fill all the octahedrally coordinated sites in the surface layer with metal atoms, as in the manner of stoichiometric FeO. The surface regions of these nanoparticles are, thus, very different from the structure of bulk Fe_3O_4.

Similar images have also been observed in other spinel-based oxides. Electron-beam induced recrystallization of α-Al_2O_3 into the γ-form, which has the defect spinel structure, has been noted (Smith *et al*. 1986), and although γ-Al_2O_3 is difficult to prepare in the pure state, there is strong thermodynamic evidence that, as the particle size decreases, it becomes the thermodynamically stable structure (McHale

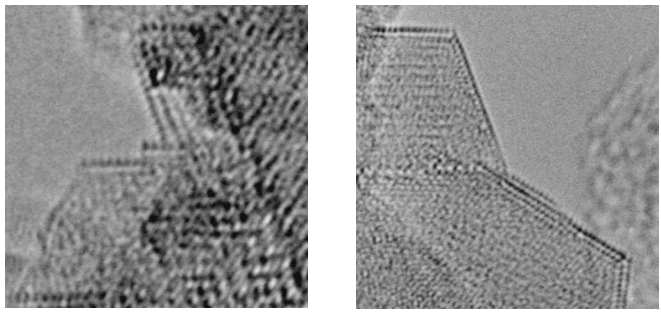

(*a*) (*b*)

Figure 5. Octahedral and cubeoctahedral particles of γ-Al_2O_3, showing the same enhanced surface contrast as that observed in the iron oxides.

et al. 1997). Al_2O_3 is widely used as a support for metal catalysts, and it is believed that the 'active' support, which facilitates the monodispersion of metals, is in fact the γ-form. Images of particles of γ-Al_2O_3 are shown in figure 5*a*, *b*. That in figure 5*a* is at the higher end of the nanoparticle size regime, but still shows strong contrast at the edges, with only weak fringe contrast in the interior regions. The only difference from Fe_3O_4 is the truncation of the {100} faces so that the overall particle shape is octahedral. In the smaller particle shown in figure 5*b*, the central fringe contrast is almost entirely absent and the interior appears to be amorphous. These images can be interpreted using the same model as Fe_3O_4, using metal atom terminations and an excess of metal vacancies in the interior (Jefferson *et al*. 1992). In addition, because of the reduced difference in the scattering powers of oxygen and aluminium, the enhanced contrast at the particle edges can only be explained if the surface is truly metal terminated, with no outer oxygen atoms. Bearing in mind the reactivity of aluminium, this is chemically very surprising, but it may explain the ease with which metals such as platinum and rhenium disperse when supported on γ-Al_2O_3, as when these metals are added to a specimen of γ-Al_2O_3 nanoparticles they can 'dissolve' in the surface metal layer and release aluminium ions that migrate to the particle interior, further stabilizing the particle. The exact valence of metal atoms added in this way has not yet been determined, but it is unlikely to be zero, explaining the extreme reactivity of such catalysts.

5. New oxide structures in nanoparticle form

The nanoparticles described above are modified variants of bulk structures. Given the influence of surface-energy considerations, however, the possibility exists of new structures in nanoparticles that have no bulk counterpart. A phase of this type has recently been found in tungsten trioxide. There are three reported structures for tungsten trioxide, one of which, m-WO_3, is a perovskite network of corner-sharing WO_6 (Wells 1984), and two further structures which have been prepared using 'wet' methods, namely a simple hexagonal form, h_1-WO_3, and a pyrochlore-like form, p-WO_3 (Figlarz 1989). Both of the latter contain tunnels formed by six WO_6 octahedra, and convert irreversibly to m-WO_3 at temperatures above 700 K (Gerand *et al*. 1979). The hexagonal form is basically a pure oxide equivalent of some alkali tungsten

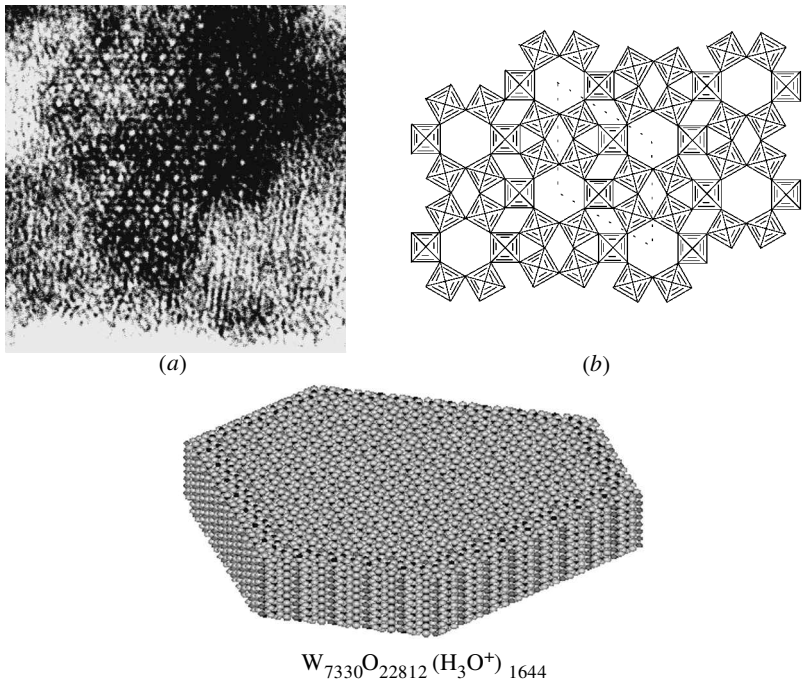

Figure 6. The new form of WO_3. (*a*) High-resolution electron micrograph of a nanoparticle of h_2-WO_3. (*b*) Structural model of the new phase. (*c*) Schematic of the nanoparticle as a large polyanion. Tungsten atoms are represented by the small dark circles, with H_3O^+ ions as small, lighter circles. Once again, oxygen atoms are represented by the larger circles. The particle stoichiometry is $W_{7330}O_{22812}(H_3O^+)_{1644}$.

bronzes (Ekstrom & Tilley 1980), although the thermodynamic stability of h_1-WO_3 and p-WO_3 is open to question.

Nanoparticles of WO_3 may be prepared using sol-gel techniques from acidified sodium tungstate followed by refluxing with either 30% H_2O_2 or NH_4Cl solution at a higher pH until a fine yellow precipitate forms (Tilley 1997). Specimens produced in this way show particles with both the m-WO_3 and h_1-WO_3 structures, but also nanoparticles of a new phase, also hexagonal, but with a much larger unit cell than that of h_1-WO_3 (Tilley & Jefferson 1999). A micrograph of a particle of this phase is shown in figure 6*a*, and a schematic diagram of the structure, which has been confirmed from image simulations in figure 6*b*. This phase, which has been designated h_2-WO_3, is intermediate between the known monoclinic and hexagonal forms, in that it contains the hexagonal tunnels of the latter separated by groups of four octahedra from the former. A similar configuration has been observed in bulk specimens of $Sb_{0.2}WO_3$, although in the latter the separation of the hexagonal tunnels by elements of the m-WO_3 structure is only in one direction (Dobson *et al.* 1987). It is believed that the tunnels of the h_1-WO_3 structure form around H_3O^+ ions which are present at low pH: raising the pH effectively reduces their concentration and ensures that the monoclinic structure begins to form. At intermediate pH values, however, the hexagonal tunnels will still form but their overall density is reduced, and the

space between them is filled with elements of the monoclinic structure. A whole series of intermediates is, therefore, possible, but although disordered nanoparticles have been noted, only the h_2-structure has been observed in a perfect arrangement. That part of the new arrangement derived from m-WO_3 is heavily distorted and extremely strained, and it is probable that in bulk specimens such strain could not be accommodated. In the original solution, these nanoparticles are almost certainly gigantic large polyanions of the type shown in figure 6*c*, and it is therefore quite likely that other hitherto unknown structural variants can exist.

6. Conclusions

Because of the severe difficulties encountered in their characterization, our knowledge of the internal structures of non-metallic nanoparticles is only in its infancy. What has been shown to date, however, is that it is unwise to assume that these are the same as those of bulk materials, although they may be based on a known atomic configuration. It therefore follows that the properties of such particles, both physical and chemical, are unlikely to be those of the bulk and may well, like the structure itself, depend heavily on the particle size. Possibly the greatest mistake that can be made is to assume that these nanoparticles are merely small crystals: they lie in a size dimension between true crystals and conventional molecules, and their properties may resemble those of the latter. The consequences of this, particularly as these particles form a potentially intractable component of atmospheric pollution, may well be significant.

References

Amdur, M. O., Chen, L. C., Guty, J., Lam, H. F. & Miller, P. D. 1988 *Atmos. Environ.* **22**, 557–560.

Bevan, D. J. M. 1955 *J. Inorg. Nucl. Chem.* **1**, 49–59.

Bevan, D. J. M. 1973 *Comprehensive inorganic chemistry*. Oxford: Pergamon.

Brauer, G. 1964 *Progress in the science and technology of the rare earths*, vol. 1, p. 152. New York: Pergamon.

Brinker, C. J. & Scherer, G. W. 1990 In *Sol-gel science: the physics and chemistry of sol-gel processing*. Academic.

Cowley, J. M. & Moodie, A. F. 1957 *Acta Crystallogr.* **10**, 609–619.

Dobson, M. M., Hutchison, J. L., Tilley, R. J. D. & Watts, K. A. 1987 *J. Solid State Chem.* **71**, 47–60.

Ekstrom, T. & Tilley, R. J. D. 1980 *Chemica Scripta* **26**, 535–546.

Figlarz, M. 1989 *Progr. Solid State Chem.* **19**, 1–46.

Gerand, B., Nowogrocki, G., Guenot, J. & Figlarz, M. 1979 *J. Solid State Chem.* **29**, 429–434.

Gilmour, P., Brown, D. M., Beswick, P. H., Benton, E., MacNee, W. & Donaldson, K. 1997 *Ann. Occup. Hygiene* **41**, 32–38.

Gribelyuk, M. A., Harris, P. J. F. & Hutchison, J. L. 1994 *Phil. Mag.* **69**, 655–669.

Gschneider, K. A. & Eyring, L. 1979 *Handbook on the physics and chmistry of rare earths*, vol. 3. Amsterdam: North Holland.

Harris, P. J. F. 1986 *Nature* **323**, 792–794.

Heinemann, K., Yacaman, M. J., Yang, C. Y. & Poppa, H. 1979 *J. Cryst. Growth* **47**, 177–183.

Howie, A. & Marks, L. D. 1984 *Phil. Mag.* A **49**, 95.

Hutchison, J. L. 1990 *Proc. 12th Int. Congr. Electron Microscopy*, vol. 1, pp. 478–479. San Francisco Press.

Jefferson, D. A. & Harris, P. J. F. 1988 *Nature* **332**, 617–620.

Jefferson, D. A., Kirkland, A. I., Reller, A., Tang, D., Williams, T. B. & Zhou, W. 1992 *Electron microscopy 1992*, vol. 2, pp. 611–614. Universidad de Granada.

McHale, J. M., Auroux, A., Perotta, A. J. & Navrotsky, A. 1997 *Science* **277**, 788–791.

Marks, L. D. & Smith, D. J. 1981 *J. Cryst. Growth* **54**, 425.

Marks, L. D. & Smith, D. J. 1983 *J. Microscopy* **130**, 249–261.

Morris, B. C., Flavell, W. R., Mackrodt, W. C. & Morris, M. A. 1993 *J. Mater. Chem.* **3**, 1007–1013.

Smith, D. J., Bursill, L. A. & Jefferson, D. A. 1986 *Surf. Sci.* **175**, 673–683.

Tilley, E. E. M. 1997 Synthesis and characterisation of nanocrystalline metal oxides. PhD thesis, University of Cambridge, UK.

Tilley, E. E. M. & Jefferson, D. A. 1999 *Particulate matter*, pp. 63–84. Oxford: BIOS Scientific.

Uppenbrink, J., Kirkland, A. I., Wales, D., Jefferson, D. A. & Urban, J. 1992 *Phil. Mag.* B **65**, 1079–1096.

Wells, A. F. 1984 *Structural inorganic chemistry*, 4th edn, pp. 516–573. Oxford University Press.

PHILOSOPHICAL TRANSACTIONS OF THE ROYAL SOCIETY A MATHEMATICAL, PHYSICAL & ENGINEERING SCIENCES